SUPPORTING INFORMATION

Singlet Oxygen Photogeneration in Coastal Seawater: Prospect of Large-Scale Modelling in Seawater Surface and its Environmental Significance.

Michael O. Sunday[a,b], Kazuhiko Takeda[a], Hiroshi Sakugawa[a*]

[a]Graduate School of Biosphere Science, Hiroshima University, 1-7-1, Kagamiyama, Higashi-Hiroshima, 739-8521 Japan.

[b]Department of Chemistry, Federal University of Technology, Akure, P.M.B 704, Ondo State, Nigeria. E-mail: omsunday@futa.edu.ng

*Corresponding Author

Hiroshi Sakugawa

Graduate School of Biosphere Science, Hiroshima University, 1-7-1, Kagamiyama, Higashi-Hiroshima, 739-8521 Japan. Tel: +81-82424-6504; E-mail: hsakuga@hiroshima-u.ac.jp

Total number of pages: 30

Total number of figures: 7

Total number of tables: 4

CONTENTS

S1: CDOM absorption characteristics

Absorption coefficient (a_{300})

The absorbance due to CDOM in the samples was monitored using an UV-visible spectrophotometer (UV-2400, Shimadzu, Japan). Samples were placed in a 5 cm pathlength (l) quartz cuvette and absorbance readings at 300 nm (A_{300}) were obtained. Prior to sample measurement, MilliQ water was used to obtain baseline values and was intermittently analyzed during sample measurements to check for consistency and correction where necessary. The A_{300} was then converted to the Napierian absorption coefficient (a_{300}, m^{-1}) according to equation (S1.1).[1]

$$a_{300} = \frac{2.303 A_{300}}{l} \qquad (S1.1)$$

Spectra slope

The slope of the CDOM absorption spectra, which is known as the spectra slope (S), was determined by fitting the absorption coefficient values (a_λ) from 300–550 nm to the exponential function in equation S1.2 using a non-linear least square regression routine.[1,2]

$$a_\lambda = (a_{\lambda 0} - K)e^{-S(\lambda - \lambda 0)} + K \qquad (S1.2)$$

where S is the spectra slope (µm^{-1}), a_λ is the absorption coefficient at wavelength λ, $a_{\lambda 0}$ is the absorption coefficient at reference wavelength λ_0 (300 nm) and K is a constant to account for baseline offset.

Carbon-specific absorption (a*300)

36

37 The carbon-specific absorption or specific absorption coefficient (a^*_{300}) is defined as the

38 absorption coefficient (a_{300}) normalized to DOC concentration (mg C/L) of the sample.[3] The units

39 are $m^2\ g^{-1}$ C. This variable also provides information regarding variations in CDOM composition

40 as it shows how "chromophoric" the DOC content of a sample is. Additionally, this variable has

41 been shown to have a positive correlation with aromatic content and molecular size of DOC.[4]

S2: Photoirradiation experiments

42

Laboratory irradiation under a solar simulator

43

44 Solutions to be irradiated (7 mL) were contained in an 8.8 mL quartz cell and irradiated under a

45 solar simulator. The device consisted of a lamp housing (WACOM Co., HX-500) equipped with a

46 500 W Xe lamp (WACOM Co., KXL-500F) and an optical filter (HOYA Co., UV-31) with a

47 transmission wavelength limit of 310 nm. The quartz cell was placed in an air-conditioned

48 compartment of the simulator that maintained the temperature of the sample at 20°C during

49 irradiation. A detailed description of the solar simulator has been reported by Nakatani et al.[5]

50 Aliquots were withdrawn at intervals for HPLC analysis.

S3. Analytical determinations

51

S3A. Singlet oxygen

52

53 $^1O_2$ was determined using FFA as a chemical probe. Samples were spiked with FFA (final

54 concentration; 100 μM) and irradiated under a solar simulator or sunlight accordingly. At intervals,

55 aliquots of the reaction mixture were withdrawn and analyzed for FFA and 6-HP-one simultaneously

56 by HPLC. The isocratic HPLC system consisted of a pump (Prominence LC-20AD, Shimadzu,

57 Kyoto) that delivered *eluent* (0.1% H_3PO_4: ACN (90:10)) at a flow rate of 1 mL/min, as well as an

58 injection valve equipped with a 20 µL sample loop for sample injection. FFA and 6-HP-one were

59 separated on a C_{18} column (Cosmosil, MS-II, 250 mm x 4.6 mm, 5 µm) and detected on a UV-

60 Visible detector (Prominence LC-20AD, Shimadzu, Kyoto, Japan) at 219 nm.

61 *Kinetic data treatment*

62 Generation of $^1O_2$ using FFA as a probe was determined by monitoring: (i) FFA degradation (HH

63 method) and (ii) 6-HP-one formation (ZM method) adopting the approach used by Zhou and

64 Mopper.[6]

65 *HH method*

66 FFA reacts with $^1O_2$ resulting in a pseudo first order degradation rate constant, k, of FFA. As

67 shown in Fig. S4, the degradation of FFA in this study also followed first order kinetics. Therefore,

68 $[^1O_2]_{ss}$ was be determined from equation S3.1 by dividing the observed first order degradation rate

69 constant (k) of FFA in the irradiated solution by the reaction rate constant of FFA with $^1O_2$

70 ($k_{FFA,1O2}$), which is given as 1.09×10^8 $M^{-1}s^{-1}$.[7] The $k_{FFA,1O2}$ used for each sample was corrected

71 for the effect of salinity on the rate constant as recommended by Appiani et al.[8]

72
$$[^1O_2]_{ss} = K/k_{FFA,^1O_2} \quad (S3.1)$$

73 The photoformation rate (R^1O_2) was calculated using equation S3.2:

74
$$R^1O_2 = [^1O_2]_{ss} \times k_d \quad (S3.2)$$

75 where k_d is the dissociation rate constant of $^1O_2$ in water given as 2.5×10^5 s^{-1}.[9] Water is the main

76 scavenger of $^1O_2$; hence, the scavenging capacity of other potential scavengers in natural waters

77 are negligible.

78

ZM method

The photoformation rate of $^1O_2$ (R^1O_2) was also investigated using the approach described by Zhou and Mopper[6] by monitoring 6-HP-one formation. It was determined using equation S3.3, where $R_{6\text{-HP}}$ is the formation rate of 6-HP-one from the reaction of FFA and $^1O_2$; $Y_{6\text{-HP}}$ is the yield of 6-HP-one defined as the amount of 6-HP-one formed for each mole of FFA that reacts with $^1O_2$ and F is the fraction of $^1O_2$ that reacts with FFA. $Y_{6\text{-HP}}$ was determined using equation S3.4.

$$R_{^1O_2} = \frac{R_{6-HP}}{Y_{6-HP} \ \ x \ F} \quad (S3.3)$$

$$Y_{6-HP} = \frac{photoformation \ rate \ of \ 6 - HP - one}{degradation \ rate \ of \ FFA} \quad (S3.4)$$

The reaction of FFA and $^1O_2$ in the sample is in competition with the deactivation or quenching of $^1O_2$ by water as the main quencher of $^1O_2$. Therefore, the fraction, F, which is the fraction of $^1O_2$ that reacts with FFA, compared to physical quenching by H_2O molecules was obtained using equation S3.5:

$$F = \frac{k_{FFA,^1O_2} \ [FFA]}{k_d \ + \ k_{FFA,^1O_2} \ [FFA]} \quad (S3.5)$$

The value of F varied slightly between 0.0368–0.0372 due to the salinity correction applied to the $k_{FFA,1O2}$.

S3B. ·OH determination

·OH photoformed in the seawater sample was measured using benzene as a chemical probe.[10,11] Briefly, 7 mL samples were spiked with a final concentration of 1.2 mM benzene and irradiated

97   using the solar simulator described above. The same quartz cell used for the $^1O_2$ irradiation

98   experiment above was also used here. The irradiation lasted for about 40 mins, during which time

99   aliquots were obtained at 10 min intervals for phenol determination using an HPLC.

100   The HPLC system used for this determination consisted of a pump (LC-10A$_i$, Shimadzu, Kyoto,

101   Japan) that delivered eluent (acetonitrile:MQ (60:40)) at a flow rate of 1 mL/min. An injection

102   valve equipped with a 50 µL sample loop was used to inject samples into the system. Phenol was

103   separated on a C$_{18}$ column (Cosmosil, MS-II, 250 mm x 4.6 mm, 5 µm) and detected using a

104   fluorescence detector (LC-20AD, Shimadzu, Kyoto, Japan) set at excitation/emission wavelengths

105   of 270/298 nm.

106   The photoformation rate of ·OH (ROH) was determined using equation S3.6:

107
$$R_{OH} = \frac{R_{phenol}}{Y_{phenol} \; x \; F_{benzene-OH}} \qquad (S3.6)$$

108   where Rphenol is the photoformation rate of phenol in each irradiated sample; Y$_{phenol}$ is the yield

109   of phenol formed in the reaction between benzene and ·OH, and F$_{benzene-OH}$ is the fraction of ·OH

110   that reacts with benzene during the irradiation of benzene-spiked samples. A Y$_{phenol}$ of 0.75

111   reported by Arakaki & Faust[10] and an F$_{benzene-OH}$ value of 0.68 reported in Seto inland seawater by

112   Takeda et al.[11] were used for all calculations.

113   The generated ·OH will be scavenged by both benzene and the group of all other potential

114   scavengers such as DOM and Br$^-$, in seawater. Hence, it is important to determine the scavenging

115   rate constant (SRC) of these scavengers in the seawater sample. The SRC is the sum of the reaction

116   rates (rate constant of scavenger with ·OH (k$_{s,OH}$) x [Scavengers]) given as $\sum_i^j \left(k_{si,OH}\right)[s]$ of all

117   other scavengers present in the seawater sample that compete with benzene for the photoformed

118   ·OH.

119   The SRC was determined using equation S3.7, which expresses the fraction ($F_{benzene-OH}$) of ·OH

120   that reacts with benzene.

121
$$F_{benzene-OH} = \frac{k_{benzene-OH}\,[benzene]}{k_{benzene-OH}\,[benzene]\ +\ \sum_{i}^{j}(k_{si,OH})[s]} \quad (S3.7)$$

122   where $k_{benzene-OH}$ is the reaction rate constant of benzene with ·OH given as 7.8 x 10^9 M^{-1} s^{-1}.[12]

123   By substituting equation S3.7 for $F_{benzene-OH}$ in equation S3.6 and making R_{phenol} the subject of the

124   formula, the following equation was obtained:

125
$$\frac{1}{R_{phenol}} = \frac{1}{R_{OH}Y_{OH}} + \frac{\sum_{i}^{j}(k_{si,OH})[s]}{R_{OH}Y_{OH}k_{benzene-OH}}\ x\ \frac{1}{[Benzene]} \quad (S3.8)$$

126   Therefore, a plot of 1/R$_{phenol}$ against 1/[Benzene] gives a straight-line graph with:

127    $Intercept = \frac{1}{R_{OH}Y_{OH}}$; $Slope = \frac{\sum_{i}^{j}(k_{si,OH})[s]}{k_{benzene-OH}}\ x\ Intercept$

128   Hence, SRC ($\sum_{i}^{j}(k_{si,OH})[s]$) $= \frac{Slope\ x\ k_{benzene-OH}}{Intercept}$ $\quad (S3.9)$

129   To determine SRC experimentally, seawater samples were treated with varying concentrations of

130   benzene (25, 50, 75 and 100 µM) and irradiated, after which their corresponding R$_{phenol}$ values

131   were obtained. A plot of 1/R$_{phenol}$ against 1/[Benzene] gave a straight-line graph as expected from

132   equation S3.8. The slope and intercept obtained in addition to $k_{benzene-OH}$ were then used in equation

133   S3.9 to obtain the SRC for the sample.

134   The steady state concentration [·OH]ss was determined using equation (S3.10)

$$135 \qquad [^{\cdot}OH]_{ss} = \frac{Photoformation\ rate, R_{OH}}{Scavenging\ rate\ constant} \qquad (S3.10)$$

136 Having initially obtained R_{OH}, the steady state concentration was obtained after determining the

137 SRC in each sample.

S4. Other measurements

139 Nitrite was determined according to the method described by Strickland and Parsons.[13] This

140 procedure is based on the reaction of nitrite with sulfanilamide in an acid solution to form a

141 diazonium compound, which is then coupled to N-(1-Naphthyl)-ethylenediamine dihydrochloride

142 to form a colored azo dye. The absorbance of the azo dye is then read spectrophotometrically at

143 540 nm. Sample concentrations were determined from a calibration curve obtained using standard

144 solutions of nitrite ion.

145 Dissolved organic carbon (DOC) was analyzed using a TOC-VCSH analyzer (Shimadzu, Kyoto,

146 Japan). Potassium hydrogen phthalate was used as the standard to obtain the calibration curve for

147 DOC measurement.

S5. Effect of azide on $^1O_2$ determination

149 NaN$_3$ is an effective quencher of $^1O_2$; therefore, irradiation of FFA-spiked samples in the presence

150 of NaN$_3$ is expected to result in a corresponding decrease in the rate of FFA degradation (R_{FFA})

151 and 6-HP-one formation (R_{6-HP}). To investigate this, the S11 seawater sample, which had the

152 highest CDOM abundance, was spiked with FFA and irradiated in the absence and presence of 0.5

153 mM NaN$_3$. The R_{FFA} was monitored in both experiments. As shown in Fig. S4, R_{FFA} was reduced

154 in the presence of azide compared with its absence.

155   Mathematically, R_{FFA} can be expressed as:

$$R_{FFA} = R_{^1O_2} \; x \; Fraction \; (F) \quad (S5.1)$$

157   In the absence of azide, F is obtained from equation S5.2 as shown below.

$$F = \frac{k_{FFA,^1O_2} \, [FFA]}{k_d + k_{FFA,^1O_2} \, [FFA]} \quad (S5.2)$$

$$F = \frac{1.09 \; x \; 10^8 \; x \; 1x10^{-4}}{2.76 \; x \; 10^5 + (1.09 \; x \; 10^8 \; x \; 1x10^{-4})}$$

$$F = 0.038$$

161   However, in the presence of azide, F can be expressed as equation S5.3:

$$F = \frac{k_{FFA,^1O_2} \, [FFA]}{k_d + k_{FFA,^1O_2} \, [FFA] + k_{NaN_3,^1O_2} [NaN_3]} \quad (S5.3)$$

$$F = \frac{1.09 \; x \; 10^8 \; x \; 1x10^{-4}}{2.76 \; x \; 10^5 + (1.09 \; x \; 10^8 \; x \; 1x10^{-4}) + (7.8 \; x \; 10^8 \; x \; 5 \; x \; 10^{-4})}$$

$$F = 0.0163$$

165   where $k_{NaN_3, \, ^1O_2}$ is the reaction rate constant between azide and $^1O_2$ was given as $7.8 \times 10^8 \; M^{-1} \; s^{-1}$.

166   F in the presence of azide was 0.0163, which represents a 43% reduction from the value of 0.038

167   obtained in the absence of azide. According to equation S5.1, R^1O_2 was assumed to be constant in

168   both experiments with and without azide; therefore, R_{FFA} is dependent on F. Hence, R_{FFA} in the

169   presence of azide was expected to be reduced by 43% based on the % reduction in F.

170   Experimentally, the R_{FFA} obtained in the absence of azide was 0.0288 µM/min, while that obtained

171   in the presence of azide was 0.0126 µM/min. This represents a 44% reduction in R_{FFA} in the

172   presence of azide, which agrees with kinetic estimations of 43%. These findings confirm that the

173 degradation of FFA in this study was mediated by $^1O_2$ photoformed in the irradiated seawater

174 sample.

175 The effects of azide on R_{6-HP} were also investigated. R^1O_2 determined based on R_{6-HP} can be
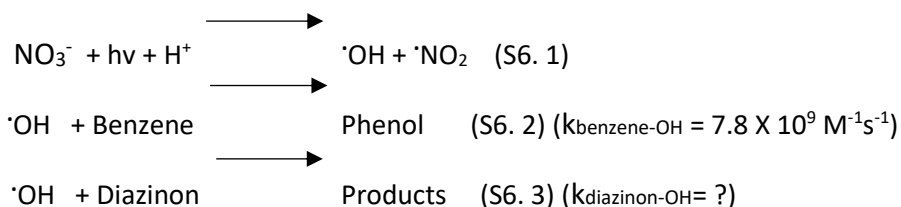
176 expressed as equation X4:

$$R_{^1O_2} = \frac{R_{6-HP}}{Y_{6-HP} \; x \; F} \qquad (X4)$$

178 Assuming R^1O_2 and Y_{6-HP} are constant in both experiments with and without azide, R_{6-HP} will be

179 dependent on F and is expected to follow a manner dependent on % reduction in F (43 %). The R_{6-}

180 $_{HP}$ in the absence of azide was 0.029 µM/min, while it was 0.014 µM/min in the presence of azide.

181 This represents a 48% reduction in agreement with kinetic estimations based on the % reduction

182 in F. This also shows that formation of 6-HP-one arose from the reaction between FFA and $^1O_2$.

183 **S6. Reaction rate constants of diazinon with ROS ($^1O_2$ and $^.OH$)**

184 • **Reaction rate constant of diazinon with $^.OH$**

185 The reaction rate constant of diazinon with $^.OH$ was investigated by the competition kinetics

186 method using benzene as a reference compound and 1 mM NO_3^- as the photochemical source of

187 $^.OH$ generation in MQ.[14] Benzene reacts with $^.OH$ to form phenol, which has a known reaction

188 rate constant of 7.8 x 10^9 M^{-1} s^{-1}.[12]

189

$NO_3^- + h\nu + H^+ \longrightarrow$ $^.OH + ^.NO_2$ (S6. 1)

190

$^.OH$ + Benzene $\longrightarrow$ Phenol   (S6. 2) ($k_{benzene-OH}$ = 7.8 X 10^9 $M^{-1}s^{-1}$)

191

$^.OH$ + Diazinon $\longrightarrow$ Products   (S6. 3) ($k_{diazinon-OH}$= ?)

192   When a solution containing NO_3^- and benzene in MQ is irradiated in the absence of diazinon, all

193   of the generated ·OH reacts with benzene (S6.2) to give phenol product. However, in the presence

194   of diazinon, the generated ·OH reacts with both benzene and diazinon. In this case, the observed

195   phenol product is expected to be lower. This reduction is because of competition of the reaction of

196   diazinon with the generated ·OH.

197   The relationship between phenol produced in the absence and presence of diazinon can be

198   expressed according to equation S6.4 below:

199    $$\frac{R_{phenol}}{R'_{phenol}} = 1 + \frac{k_{diazinon-OH}[diazinon]}{k_{benzene-OH}[benzene]} \quad (S6.4)$$

200   where R_{phenol} and R'_{phenol} are the phenol signals in the absence and presence of diazinon,

201   respectively, and $k_{benzene-OH}$ and $k_{diazinon-OH}$ are the reaction rate constants of benzene with ·OH and

202   diazinon with ·OH, respectively.

203   Based on equation S6.4, a plot of R_{phenol}/R'_{phenol} against [diazinon]/[benzene] should give a straight

204   line with an intercept of 1 and a slope = $k_{diazinon-OH}/k_{benzene-OH}$. Experimentally, the rate of phenol

205   production in the absence of diazinon and its rate in the presence of varying concentrations of

206   diazinon was obtained and plotted against the [diazinon]/[benzene] ratio.

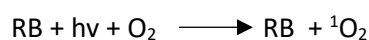207   *Procedure*

208   A stock solution of 30 mg/L (98.6 µM) diazinon was prepared by dissolving in MQ. The solubility

209   limit of diazinon in water according to the literature is 40 mg/L. A solution containing 200 µM

210   benzene and 1 mM NO_3^- (as the photochemical source of ·OH generation) was irradiated in the

211   absence of diazinon for 20 min. The phenol signal obtained was taken as R_{phenol}. Subsequently, a

212   solution containing the same concentration of benzene and NO_3^- was irradiated in the presence of

213   varying concentrations of diazinon (5, 10, 30 and 50 µM). The phenol signal here was taken as

214   R'_{phenol}. The concentrations of benzene and diazinon were selected such that the

215   [diazinon]/[benzene] ratio was ≤1. The phenol produced from the irradiated solutions was

216   determined by HPLC. A plot of R_{phenol}/R'_{phenol} against [diazinon]/[benzene] is shown in Fig. S6.

217   The HPLC system used in the determination of phenol consisted of a pump (LC-10A$_i$, Shimadzu,

218   Kyoto, Japan) that delivered eluent (acetonitrile:MQ (60:40)) at a flow rate of 1 mL/min. An

219   injection valve equipped with a 50 µL sample loop was used to inject samples into the system.

220   Phenol was separated on a C_{18} column (Cosmosil, MS-II, 250 mm x 4.6 mm, 5 µm) and detected

221   using a fluorescence detector (RF-10A$_{XL}$, Shimadzu, Kyoto, Japan) set at excitation/emission

222   wavelengths of 270/298 nm.

223   • **Reaction rate constant of diazinon with $^1O_2$**

224   The reaction rate constant of $^1O_2$ with diazinon was determined by monitoring the degradation rate

225   of diazinon as it reacted with excessively high [$^1O_2$] generated using Rose Bengal as a

226   sensitizer.[15,16]

227                     $RB + hv + O_2 \longrightarrow RB + {}^1O_2$

228                     $Diazinon + {}^1O_2 \longrightarrow Products$ ($k_{diazinon-{}^1O_2}$)

229   Rate of diazinon degradation (R_{deg}) = $k_{diazinon-{}^1O_2}$[diazinon][$^1O_2$]   (S6.5)

230   where $k_{diazinon-{}^1O_2}$ is the reaction rate constant of diazinon with $^1O_2$. At constant [$^1O_2$], R_{deg} was

231   directly proportional to the [diazinon]. Therefore, as [diazinon] increases, R_{deg} was expected to

232   increase.

233 Moreover, when diazinon reacted with $^1O_2$, R_{deg} could be expressed as the product of rate of $^1O_2$

234 generation (R^1O_2) and fraction (F) of $^1O_2$ that reacts with diazinon as shown in equation S6.6

235 below.

$$R_{deg} = R_{^1O_2} \text{ x Fraction (F)} \qquad (S6.6)$$

236

$$F = \frac{k_{diazinon-^1O_2}[diazinon]}{k_d + k_{diazinon-^1O_2}[diazinon]} \qquad (S6.7)$$

237

238 where k_d is the dissociation rate constant of $^1O_2$ in water $= 2.5 \times 10^5 \text{ s}^{-1}$.[9]

$$R_{deg} = R_{^1O_2} \; x \; \frac{k_{diazinon-\;^1O_2}[diazinon]}{k_d + k_{diazinon-\;^1O_2}[diazinon]} \qquad (S6.8)$$

239

240 At low concentrations of diazinon (μM range), $k_{diazinon-\;^1O_2}$[diazinon] $<< k_d$, giving rise to equation

241 (S6.9):

$$R_{deg} = R_{^1O_2} \; k_d^{-1} \; k_{diazinon,^1O_2}[diazinon] \quad (S6.9)$$

242

243 Therefore, from equation S6.9, obtaining a plot of R_{deg} against [diazinon] at constant $^1O_2$

244 generation (R^1O_2) will give a slope $= R_{^1O_2} \; k_d^{-1} \; k_{diazinon-\;^1O_2}$. Since k_d is known, R^1O_2 can be

245 obtained using FFA under the same experimental conditions. A plot of R_{deg} against [diazinon]

246 where the slope $= R_{^1O_2} \; k_d^{-1} \; k_{diazinon-\;^1O_2}$ is shown in Fig. S7.

247 R^1O_2 was determined from the initial degradation rate of FFA (R_{FFA}) by equation S6.10:

$$R_{FFA} = R_{^1O_2} \; x \; \frac{k_{FFA,^1O_2}[FFA]}{k_d + k_{FFA,^1O_2}[FFA]} \qquad (S6.10)$$

248

249 where $k_{FFA, 1O2}$ is the reaction rate constant between FFA and $^1O_2$ given as $1.09 \times 10^8 \text{ M}^{-1} \text{ s}^{-1}$.[7]

250   *Procedure*

251   Mixtures of 10 µM Rose Bengal (as a $^1O_2$ photosensitizer) and varying concentrations of diazinon

252   (5, 10, 25 and 50 µM) were irradiated for about 4–6 hours using the solar simulator described

253   above. At intervals, aliquots of reaction mixture were obtained and analyzed for diazinon on HPLC

254   to monitor diazinon degradation. The HPLC system used consists of a pump (Prominence LC-

255   20AD, Shimadzu, Kyoto) that delivered eluent (ACN:MQ (80:20)) at a flow rate of 1 mL/min, as

256   well as an injection valve equipped with a 100 µL sample loop for sample injection. Diazinon was

257   separated on a C_{18} column (Cosmosil, MS-II, 250 mm x 4.6 mm, 5 µm) and detected on a UV-

258   Visible detector (Prominence LC-20AD, Shimadzu, Kyoto, Japan) at 247 nm.

259   Subsequently, the rate of $^1O_2$ generation (R^1O_2) from the irradiation of 10 µM RB as

260   photosensitizer was determined using FFA (100 µM) as a probe. The degradation of FFA because

261   of reaction with $^1O_2$ was monitored using HPLC. The HPLC system has been described earlier in

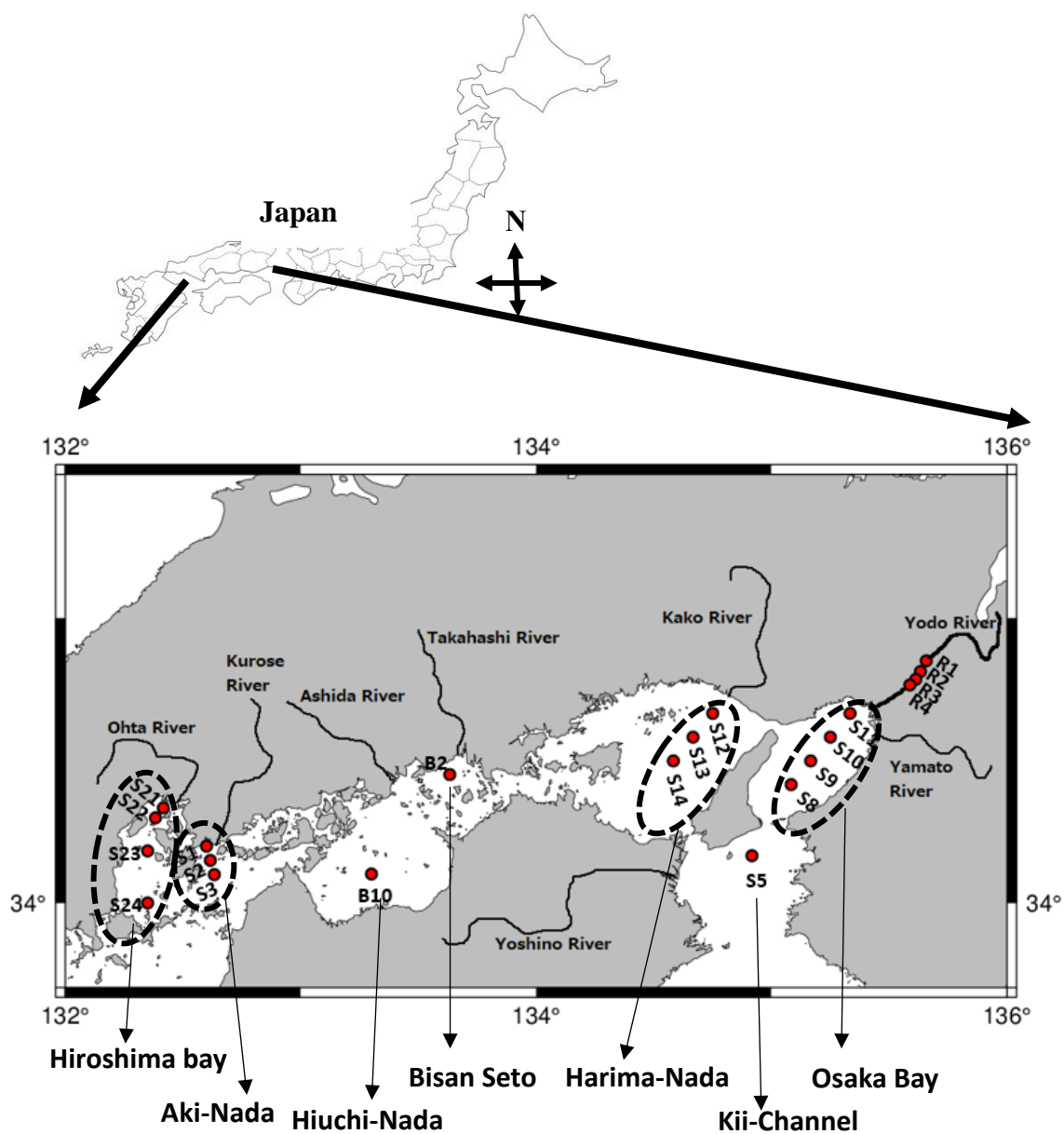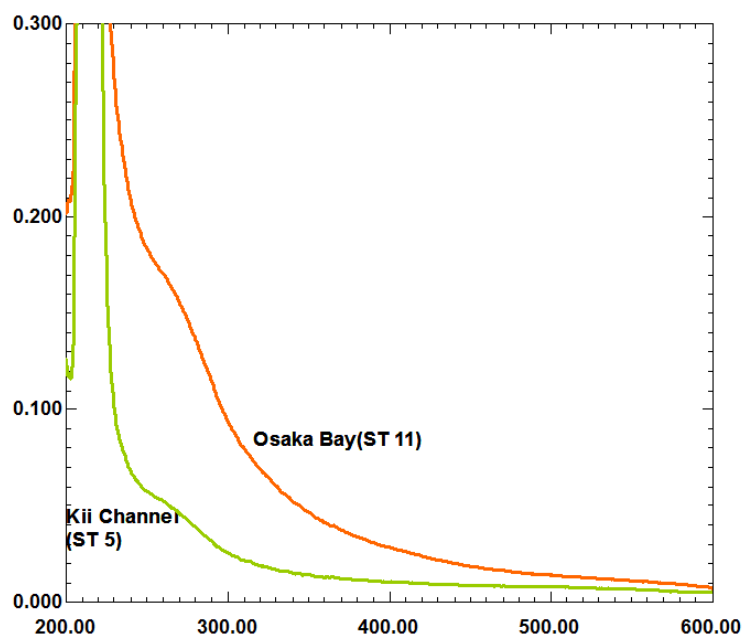262   S3A.

263

264

265

266

267

268

269

270

271

272

273

274

275

276

277

278

279

280

281

282

283

284

Figure S1: Map showing sampling stations in Seto Inland Sea and Yodo river.

285

286

287
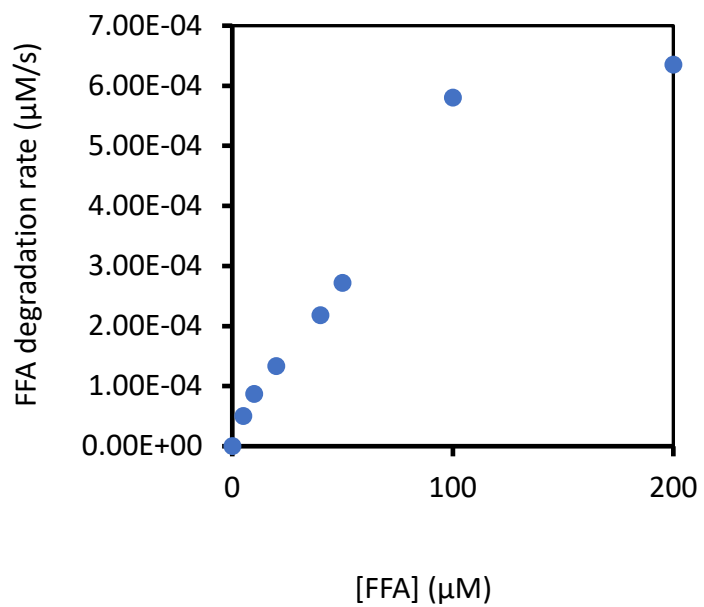
288

289   CDOM absorption

290

291   Figure S2: Absorption spectra of Kii Channel and Osaka Bay seawater sample.
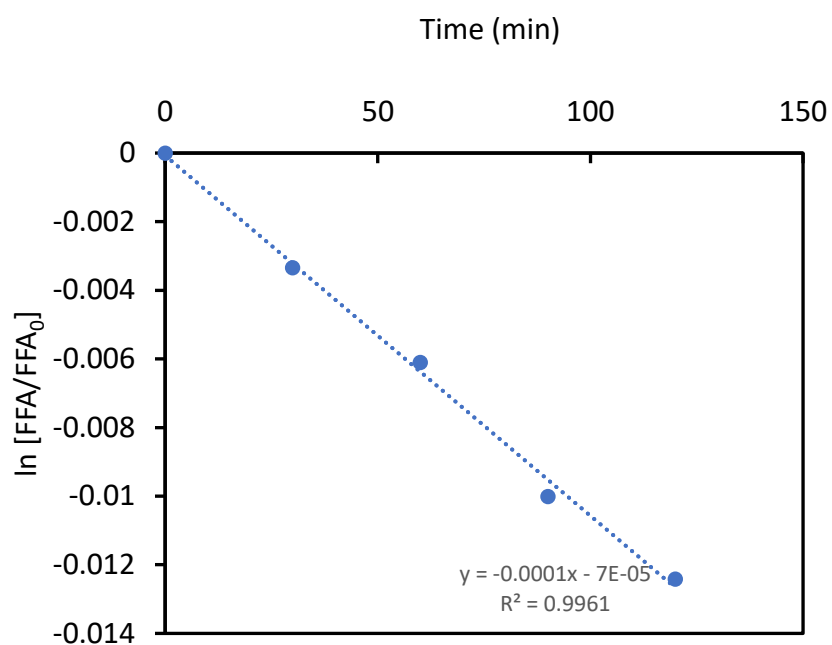
292

293

294

295

296   Figure S3: Plot of FFA degradation rate at varying [FFA] upon irradiation in seawater.

297

298

299

Figure S4: A typical first order degradation plot of FFA in an irradiated seawater sample

300

301

302

303
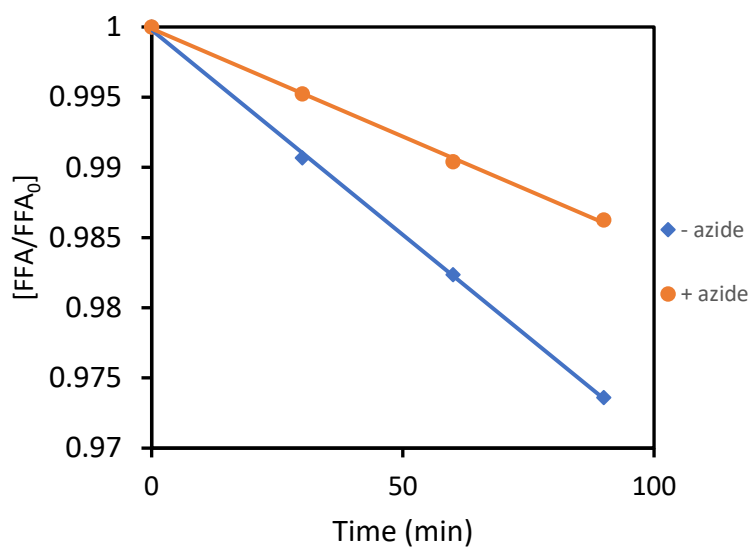
304

305   Figure S5: Effect of NaN$_3$ on FFA degradation

306

307

The plot shows a linear fit with equation:

$$y = 1.3055x + 1.0097$$
$$R^2 = 0.9995$$

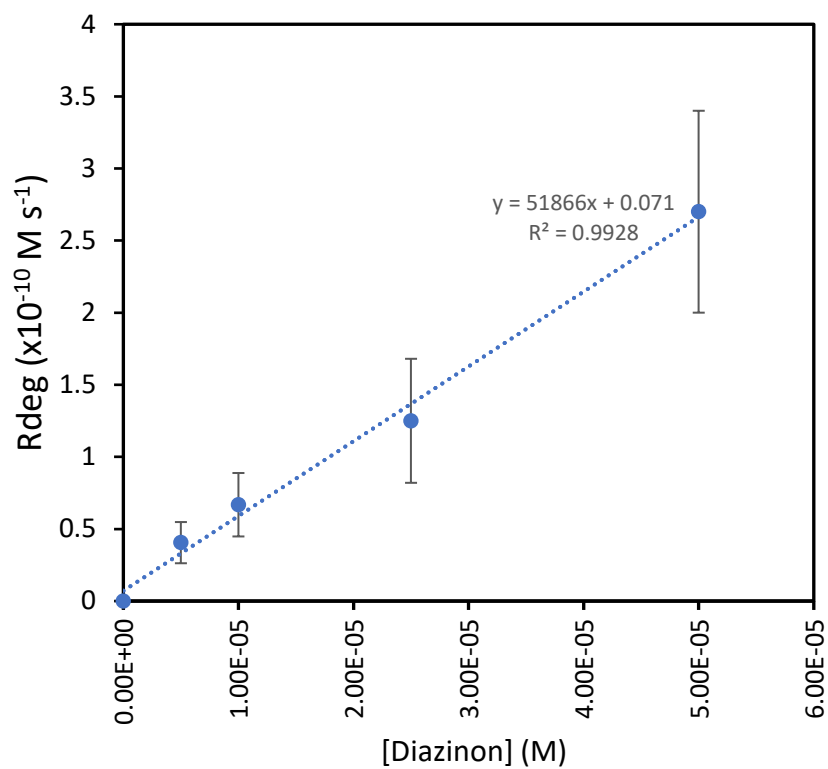with y-axis labeled "Rphenol/R'phenol" and x-axis labeled "[Diazinon]/[Benzene]".

308
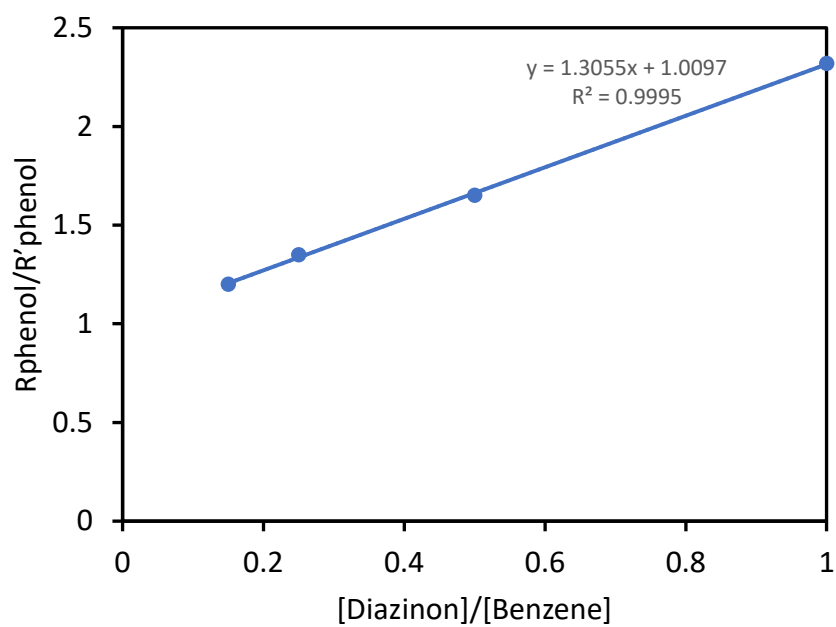
Figure S6: Plot of Rphenol/R'phenol at varying ratios of [diazinon]/[benzene].

310

311

312

313

314   Figure S7: Plot of degradation rate (R_{deg}) of diazinon at varying [diazinon].

315

316   .

Table S1: CDOM and spectra slopes reported in this and previous studies

Study Area	CDOM (m⁻¹)	*Spectra slope (S, μm⁻¹)	Wavelength range of S	Method to Obtain S	Reference
Seto Inland Sea	**a300 (0.6-3.8)**	**14.8-25**	**300-550**	**NLF**	**This study**
Carribean Sea and Orinoco River plume	Sea: a300 (0.93-2.09). River/River impacted: a300 (2.81-9.03)	I. 11-16 II. 14-22 III. 13-20	I. 400-500 II. 290-DL III. 290-DL	LF	17
Lake Superior	a300: Open lake (0.9-1.9) River-impacted (2-9.9) Riverine (10-150)	All samples: 16 - 26	300 – 600	NLF	1
Seto Inland Sea	**a355 (0.14-1.57)**			**NLF + B**	**This study**
South Pacific Ocean	a355 (0.117-0.326)	Avg. 17.3		Calculated	18
Gulf of Mexico: Open Ocean					
Spring	a355 (0.19)	15	290-DL	LF	19
Fall	(0.17)	24	290-DL		

Delaware Bay Mouth (August)	a355 (0.85)	Avg. 16	290-DL	LF	20
Tyrrhenian Sea				LF	
Coastal	a355 (0.57)	12.5	270 – DL		21
Offshore	(0.19)	25.6			
Seto Inland Sea	**a375 (0.1-1.2)**			**NLF + B**	**This study**
North Sea: Surface					2
Coastal	a375 (0.26-1.51)	Avg. 18.8	300 – 650	NLF + B	
Danish Fjords (Salinty 0-27)	a375 (0.75 – 4.5)	Avg. 19	300 - 650	NLF + B	2
Arabian Sea: Surface	a375 (0.022-0.288)	ND	ND		22

*Spectra slope comparison may be somewhat difficult because it depends on the wavelength range used, as well as the method used to obtain S- either LF or NLF. LF: linear least square fit, NLF: non-linear least square fit

Table S2: CDOM absorption coefficient, spectra slope and DOC at surface(S), middle(M) and bottom (B) depth at the various sampling stations during the July, 2017 sampling exercise

| Parameter | Depth | Aki-Nada | | | Kii Channel | Osaka Bay | | | | Harima-Nada | | | Hiuchi-Nada | Bisan-Seto |
		S1	S2	S3	S5	S8	S9	S10	S11	S12	S13	S14	B10	B2
a_{300} (m^{-1})	S	1.06	0.88	0.78	0.64	0.92	1.2	2.21	3.82	2.0	1.2	1.01	0.92	1.61
	M	0.92	0.74	0.64	0.64	0.92	0.92	1.34	1.61	1.57	1.06	0.98	0.83	1.20
	B	0.78	0.69	0.55	0.28	0.74	0.92	1.11	1.29	1.15	1.06	1.01	1.01	1.52
DOC (mg C/L)	S	0.74	0.65	0.64	0.80	0.8	0.96	1.23	1.85	1.25	1.63	1.28	1.42	1.8
	M	0.74	0.56	0.46	0.68	1.21	0.9	0.97	1.17	1.17	1.30	1.48	nd	nd
	B	0.67	0.6	0.46	0.58	0.76	0.86	0.87	1.00	1.21	1.28	nd	nd	nd
$S_{300-500}$ (µm^{-1})	S	14.7	14.5	16.4	21.7	15.8	16.8	16	13.4	18.8	23.7	25.2	24.3	18.1
	M	18.2	20.3	16.2	14.3	14.4	16.6	15.4	13.8	20.4	25.1	26.6	21.6	22.4
	B	20.8	20	17.5	14.4	14.7	17.6	16	15.6	24.5	26	26	20.7	21.3

*nd: not determined

Table S3: CDOM absorption parameter and experimentally-determined $[^1O_2]_{ss}$ for seawater samples (Hiroshima Bay, S21-S24) and Yodo River water sampled in August and November 2019 respectively.

Seawater (S21-24) & Yodo River (R1-4)	Depth	a_{300} (m^{-1})	Experimentally-determined $[^1O_2]_{ss}$ $(10^{-14}$ M)
ST 21	S	1.93	4.01
	M	1.47	3.34
	B	1.34	2.86
ST 22	S	1.34	3.04
	M	1.34	3.42
	B	1.24	2.71
ST 23	S	1.11	2.5
	M	1.01	2.18
	B	1.06	2.65
ST 24	S	1.11	2.19
	M	1.11	2.31
	B	0.98	2.29
Yodo River	R 1	4.59	6.9
	R 2	4.81	7.2
	R3	5.07	7.59
	R 4	4.88	7.34

Table S4: Half-lives ($t_{1/2}$) of compounds in seawater mediated by $^1O_2$ and $\cdot OH$

Compound	krxn,$^1O_2$ (M^{-1} s^{-1})	krxn,OH (M^{-1} s^{-1})	*$t_{1/2,1O2}$ (days)	$t_{1/2,OH}$ (days)	Reference for k values
Diazinon	$7.29 \pm 0.3 \times 10^4$	$1.01 \pm 0.18 \times 10^{10}$	3185	80.6	This study
Methyl mercury	1.90×10^6	1.90×10^9	122	428	24
TBBPA	3.90×10^8	4.80×10^9	0.63	186	23,25

*$t_{1/2,1O2}$ and $t_{1/2,OH}$ are half-lives calculated based on the average [$^1O_2$]$_{ss}$ of 3.28×10^{-14} M and [$\cdot OH$]$_{ss}$ of 8.96×10^{-18} M, respectively, obtained in this study.

References

(1) Peterson, B. M.; McNally, A. M.; Cory, R. M.; Thoemke, J. D.; Cotner, J. B.; McNeill, K. Spatial and Temporal Distribution of Singlet Oxygen in Lake Superior. *Environ. Sci. & Technol.,* **2012,** 46(13), 7222-7229.

(2) Stedmon, C. A.; Markager, S.; Kaas, H. Optical Properties and Signatures of ChromophoricDissolved Organic Matter (CDOM) in Danish Coastal Waters. *Estuarine, Coastal and Shelf Science*, **2000,** 51(2), 267-278.

(3) Tzortziou, M.; Zeri, C.; Dimitriou, E.; Ding, Y.; Jaffé, R.; Anagnostou, E.; Pitta, E.; Mentzafou, A. Colored dissolved organic matter dynamics and anthropogenic influences in a major transboundary river and its coastal wetland. *Limnology and Oceanography*, **2015,** 60(4), 1222-1240

(4) Chin, Y.-P.; Aiken, G.; O'Loughlin, E. Molecular Weight, Polydispersity, and Spectroscopic Properties of Aquatic Humic Substances. *Environ. Sci. & Technol.*, **1994,** 28(11), 1853-1858.

(5) Nakatani, N.; Hashimoto, N.; Shindo, H.; Yamamoto, M.; Kikkawa, M.; Sakugawa, H. Determination of photoformation rates and scavenging rate constants of hydroxyl radicals in natural waters using an automatic light irradiation and injection system. *Analytica Chimica Acta*, **2007,** 581(2), 260-267.

(6) Zhou, X.; Mopper, K. Determination of photochemically produced hydroxyl radicals in seawater and freshwater. *Marine Chemistry*, **1990**3, 0, 71-88.

(7) Haag, W. R.; Hoigne´, J. r.; Gassman, E.; Braun, A. M. Singlet oxygen in surface waters — Part I: Furfuryl alcohol as a trapping agent. *Chemosphere*, **1984**, 13(5), 631-640.

(8) Appiani, E.; Ossola, R.; Latch, D. E.; Erickson, P. R.; McNeill, K. Aqueous singlet oxygen reaction kinetics of furfuryl alcohol: effect of temperature, pH, and salt content. *Environmental Science: Processes & Impacts,* **2017,** 19(4), 507-516. https://doi.org/10.1039/C6EM00646A

(9) Rodgers, M. A. J.; Snowden, P. T. Lifetime of oxygen (O2(1.DELTA.g)) in liquid water as determined by time-resolved infrared luminescence measurements. *J. Am. Chem. Soc.* **1982**, 104(20), 5541-5543.

(10) Arakaki, T.; Faust, B. C. Sources, sinks, and mechanisms of hydroxyl radical (• OH) photoproduction and consumption in authentic acidic continental cloud waters from Whiteface Mountain, New York: The role of the Fe(r) (r = II, III) photochemical cycle. *Journal of Geophysical Research*, **1998,** 103(D3), 3487-3504.

(11) Takeda, K.; Takedoi, H.; Yamaji, S.; Ohta, K.; Sakugawa, H. Determination of Hydroxyl Radical Photoproduction Rates in Natural Waters. *Analytical Sciences*, **2004,** 20(1), 153-158.

(12) Buxton, G. V.; Greenstock, C. L.; Helman, W. P.; Ross, A. B. Critical Review of rate constants for reactions of hydrated electrons, hydrogen atoms and hydroxyl radicals ($\cdot$OH/$\cdot$O$-$ in Aqueous Solution. *Journal of Physical and Chemical Reference Data*, **1988**, 17(2), 513-886.

(13) Strickland, J. D. H.; Parsons, T. R. A practical handbook of seawater analysis, **1972,** 167, 2ND edition. Canada: Fisheries Research Board Of Canada Bulletin.

(14) Olasehinde, E. F.; Ogunsuyi, H. O.; Sakugawa, H. Determination of Hydroxyl Radical in Seto Inland Sea and its Potential to Degrade Irgarol. *IOSR Journal of Applied Chemistry*, **2012**,1(5), 07-14.

(15) Ruggeri, G.; Ghigo, G.; Maurino, V.; Minero, C.; Vione, D. Photochemical transformation of ibuprofen into harmful 4-isobutylacetophenone: Pathways, kinetics, and significance for surface waters. *Water Research*, **2013,** 47(16), 6109-6121.

(16) Vione, D.; Maddigapu, P. R.; De Laurentiis, E.; Minella, M.; Pazzi, M.; Maurino, V.; Minero, C.; Kouras, S.; Richard, C. Modelling the photochemical fate of ibuprofen in surface waters. *Water Research*, **2011,** 45(20), 6725-6736.

(17) Del Castillo, C. E.; Coble, P. G.; Morell, J. M.; López, J. M.; Corredor, J. E. Analysis of the optical properties of the Orinoco River plume by absorption and fluorescence spectroscopy. *Marine Chemistry*, **1999**, 66(1), 35-51.

(18) Shooter, D.; Davies-Col!ey, R. J.; Kirk, J. T. O. Light absorption and scattering by ocean waters in the vicinity of the Chatham Rise, South Pacific Ocean. *Mar. Freshwater Res*., **1998,** 49, 455-461, 1998.

(19) Green, S. A.; Blough, N. V. Optical absorption and fluorescence properties of chromophoric dissolved organic matter in natural waters. *Limnology and Oceanography,* **1994**, 39(8), 1903 - 1916

(20) Vodacek, A.; Blough, N. V.; DeGrandpre M. D.; Nelson, R. K. Seasonal variation of CDOM and DOC in the Middle Atlantic Bight: Terrestrial inputs and photooxidation. *Limnology and Oceanography*, **2003,** 42(4), 674-686.

(21) Seriti, A.; Russo, D.; Nannicini, L.; Del Vecchio, R.; DOC, absorption and fluorescence properties of estuarine and coastal waters of the Northern Tyrrhenian Sea. *Chemical Speciation and Bioavailability*, **1998**, 10(3), 95 – 106.

(22) Coble, P. G.; Del Castillo, C. E.; Avril, B. Distribution and optical properties of CDOM in the Arabian Sea during the 1995 Southwest Monsoon,Deep Sea Research Part II: Topical Studies in Oceanography, **1998,** 45, 10–11, 2195-2223.

(23) Han, S. K.; Bilski, P.; Karriker, B.; Sik, R. H.; Chignell, C. F. Oxidation of flame retardant Tetrabromobisphenol A by singlet oxygen. *Environ. Sci. Technol.*, **2008**, 42(1), 166-172. https://www.ncbi.nlm.nih.gov/pubmed/18350892

(24) Zhang, T.; Hsu-Kim, H. Photolytic degradation of methylmercury enhanced by binding to natural organic ligands. *Nat. Geosci.* **2010,** 3(7): 473-476. https://doi.org/10.1038/ngeo892

(25) Zhang, J.; He, S. L.; Hou, M. F.; Wang, L. P.; Tian, L. J. Kinetics of the Ozonation of Tetrabromobisphenol-A in Wastewater. *Advanced Materials Research*, **2011,** 383–390, 2945–2950. https://doi.org/10.4028/www.scientific.net/amr.383-390.2945